

# Phase diagram and universal scaling regimes of two-dimensional exciton–polariton Bose–Einstein condensates

Félix Helluin<sup>1</sup>, Daniela Pinto-Dias<sup>2</sup>, Quentin Fontaine<sup>2</sup>, Sylvain Ravets<sup>2</sup>, Jacqueline Bloch<sup>2</sup>, Anna Minguzzi<sup>1</sup>, Léonie Canet<sup>1</sup>

<sup>1</sup> *Université Grenoble Alpes, CNRS, LPMMC, 38000 Grenoble France,* <sup>2</sup> *Université Paris-Saclay, CNRS, Centre de Nanosciences et de Nanotechnologies (C2N), 91120 Palaiseau, France*

Many systems, classical or quantum, closed or open, exhibit universal statistical properties. Exciton-polariton condensates, being intrinsically driven-dissipative, offer a promising platform for observing non-equilibrium universal features. By conducting extensive numerical simulations of an incoherently pumped and interacting condensate coupled to an exciton reservoir we show that the effective nonlinearity of the condensate phase dynamics can be finely adjusted across a broad range, by varying the exciton-polariton interaction strength, allowing one to probe three main universal regimes with parameters accessible in current experiments: the weakly nonlinear Edwards-Wilkinson (EW) regime, where the phase fluctuations dominate, but the phase profile does not become rough, the strongly non-linear Kardar-Parisi-Zhang regime, where the condensate phase fluctuations grow in a superdiffusive manner leading to roughening of the phase, and a vortex-dominated phase emerging at stronger interactions, where both density and phase dynamics play significant roles. Our results provide a unified picture of the phase diagram of 2d exciton-polariton condensates under incoherent pumping, and shed light on recent experimental and numerical observations.

## I. INTRODUCTION

Universality and scale invariance are powerful concepts of statistical physics that allow one to classify the behaviors of physical systems in broad families independently of their microscopical details. Initially developed for systems at equilibrium, these concepts have been extended with success to the realm of out-of-equilibrium systems, where additional critical exponents arise to characterize the universal dynamics, and also new phenomena occur, such as self-organized criticality, where the dynamics itself drives the system to criticality without fine-tuning any external parameters.

Several universality classes have been identified in non-equilibrium critical phenomena. Among the earliest are the directed percolation universality class in the context of reaction-diffusion processes [1] or the Edwards-Wilkinson (EW) one in the context of stochastic interface growth [2]. The latter leads to non-anomalous exponents and a Gaussian distribution of fluctuations, as in thermal equilibrium, but it plays a key role also in non-equilibrium dynamics such as the Kuramoto-Sivashinsky equation [3, 4] or the deterministic complex Ginzburg-Landau equation [5] when the system has a finite size [6]. The EW universality class was also shown to emerge in exciton-polariton condensates [7–9]

Another celebrated universality class in non-equilibrium systems is the Kardar-Parisi-Zhang (KPZ) one, originally evidenced in randomly stirred fluids [10] and in the kinetic roughening of growing interfaces [11]. The corresponding dynamics was successively modeled by a stochastic continuous non-linear equation proposed by Kardar, Parisi, and Zhang [11]. KPZ processes display anomalous critical exponents and non-Gaussian distributions of the fluctuations [12, 13]. Far beyond its initial scope of application, the scale-invariant proper-

ties defining the KPZ universality class are nowadays observed in a wide variety of physical non-equilibrium phenomena, ranging from biophysics – cancer cells proliferation [14], to quantum physics: integrable spin chains [15, 16], density fluctuations of an Anderson localized wavepacket [17], as well as in phase dynamics of exciton-polariton Bose-Einstein condensates (BEC) [18].

Exciton-polariton (EP) condensates are formed in optical microcavities by the strong light-matter coupling between cavity photons and excitons (electron-hole bound pairs) which, under strong enough laser driving, results in the macroscopic occupation of a single quantum state [19]. Exciton-polariton condensates are in a non-equilibrium steady-state originating from the balance of pump and cavity losses. Given their driven-dissipative character, EP condensates differ radically from their equilibrium counterparts, and provide a new experimental opportunity to explore non-equilibrium universality classes. Remarkably, their universal features are directly observable from the condensate correlation functions, routinely measured in experiments.

In the one-dimensional (1d) geometry, exciton-polaritons have been identified to belong to the KPZ universality class [20, 21] through the scaling properties of the condensate two-point correlation function in space and time [7, 22], as well as through the identification of the KPZ universality subclasses in the distribution of phase fluctuations [22, 23]. KPZ universal features were experimentally observed in an incoherently pumped condensate realized on a 1d lattice of micropillars [24]. At variance with a classical interface, the KPZ regime in exciton-polaritons can be hindered by the compact nature of the phase, whose  $2\pi$ -periodicity renders possible the formation of topological phase defects, such as space-time vortices or solitons, leading to a rich phase diagram [25, 26].

In two-dimensional (2d) systems, even more scenarios for EP universal behavior have been put forward. As specific of the 2d geometry, a phase transition analogous to the Berezinskii–Kosterlitz–Thouless (BKT) one [27, 28] may arise, between a quasi-ordered phase of bounded vortex-antivortex pairs, and a disordered phase of freely moving vortices. These phases are characterized respectively by algebraic and exponential decays of the condensate spatio-temporal correlation function. This algebraic decay was reported in experiments in quasi-equilibrium EP polaritons [29]. In non-equilibrium conditions, the binding-unbinding transition of vortex-antivortex pairs has been studied theoretically building a non-linear electrodynamics analogy between vortices and charges [30, 31]. This has led to an estimate of the lengthscale  $L_v$ , separating attractive from repulsive interactions between vortex-antivortex pairs, as a function of the microscopic parameters [31]. This behavior was confirmed numerically [32, 33], and microscopic parameters such as the driving intensity are known to play a crucial role in this transition [29, 34, 35]. Numerical studies of EP BECs close to the condensation threshold also report power-law behavior of correlations with an exponent different from the equilibrium one [34].

A KPZ regime may also be found in 2d exciton-polaritons, although the conditions for achieving it are not trivial. In isotropic homogeneous incoherently pumped EP BECs, the condensate is dominated by vortex proliferation which destroys the KPZ phase [36, 37]. Numerical simulations have displayed the emergence of a KPZ regime in idealized conditions, *i.e.* in the low noise limit and in the absence of polariton-polariton interactions [8], or in the presence of a lattice, which introduces a cutoff length to vortices with smaller cores thereby taming the proliferation of both spatial and space-time vortices [23]. The KPZ regime has also been predicted to occur in anisotropic condensates [36, 38–40]. Other pumping schemes such as coherent driving [37] or the optical parametric oscillator regime (OPO) [41] also display KPZ features.

The goal of this work is to conciliate the above scenarios for 2d exciton-polaritons and propose a unified view of the possible universal regimes under experimentally relevant conditions. Specifically, we consider 2d incoherently driven polariton condensates, realized on an isotropic discrete lattice and subject to interactions, which we study using extensive numerical simulations. The inclusion of this last effect in the model is not anodyne, since it gives rise to effective attractive interactions between polaritons that lead to instabilities and reduced coherence [42]. In order to circumvent this effect, polariton condensates can be formed in a negative mass band resulting from the coupling of optical micropillars [43], which stabilizes the condensate and allows for large spatial coherence [42]. Indeed, this setting allowed for the observation of KPZ universality in the 1d system [24]. Similarly, our numerical simulations are performed setting the polaritons effective mass to a negative value.

We identify as tuning parameter the reservoir-polariton interaction energy, and show that when increasing its value three different regimes are achieved: the Edwards-Wilkinson, Kardar-Parisi-Zhang and vortex phases. We then provide a detailed characterization of these three regimes. In particular, our analysis highlights the possibility of experimental observation of the EW regime, characterized by power-law decay of space and time correlations, for which we predict specific ratios of spatial and temporal power-law exponents, which are different from the equilibrium BKT case. The EW regime is the precursor of the KPZ phase, as it emerges at small non-linearities on time and length scales where KPZ fluctuations do not yet build up [44]. Our analysis hence suggests a path towards the experimental observation of KPZ phase. Finally, we comparatively show the properties of the vortex phase highlighting the important differences with respect to the other two phases.

The paper is organized as follows. The model studied, which is the generalized Gross-Pitaevskii equation (gGPE) coupled to a rate equation for the excitonic reservoir, is introduced in Sec. II. We then review the different universal regimes in Sec. III. Our results are presented in Sec. IV, where we identify, and characterize in details the three distinct universal regimes, through the first-order correlation function and its dependence on the system size, phase statistics and momentum distribution.

## II. MODEL FOR THE CONDENSATE DYNAMICS

Under incoherent pumping, the dynamics of a 2d weakly interacting exciton-polariton condensate can be modeled by a generalized Gross-Pitaevskii equation (gGPE) for the condensate wavefunction  $\psi$  [45, 46], Eq. (1). The incoherent laser driving fills high energy bands, and the condensate is indirectly populated through an excitonic reservoir of density  $n_R$  [42, 45, 47]. This process is modeled by coupling the gGPE describing the condensate dynamics to a rate equation for  $n_R$  Eq. (2), where the excitonic reservoir is incoherently driven at pumping rate  $P$ , scatters with polaritons with amplitude  $R$ , and dissipates through other decay channels at rate  $\gamma_R$ . The complete set of dynamical equations reads

$$i\hbar\partial_t\psi = \left[ \mathcal{F}^{-1} \left[ \epsilon_{\hat{\mathbf{k}}} - \frac{i\hbar}{2}\gamma_\ell(\hat{\mathbf{k}}) \right] + \frac{i\hbar R}{2}n_R + \hbar g|\psi|^2 + 2\hbar g_R n_R \right] \psi + \hbar\xi \quad (1)$$

$$\partial_t n_R = P - (\gamma_R + R|\psi|^2)n_R, \quad (2)$$

where  $\mathcal{F}^{-1}$  denotes the inverse Fourier transform, with  $\epsilon_{\hat{\mathbf{k}}}$  the dispersion relation on the lower-polariton (LP) branch. Two-dimensional polariton condensates can be

realized on honeycomb lattices [42], where the LP branch takes on the characteristic shape of the graphene dispersion relation. Populating the condensate at the  $\Gamma$  point of the Brillouin zone, around  $\hat{\mathbf{k}} = \mathbf{0}$ , the condensate dispersion relation is well approximated by the parabola  $\epsilon_{\hat{\mathbf{k}}} = \hbar^2 \mathbf{k}^2 / (2m)$  where  $m$  is the (negative) polaritonic effective mass. It can be measured from the full imaging of the LP branch before the condensation threshold. Similarly, the momentum-dependent polariton loss rate  $\gamma_\ell(\hat{\mathbf{k}})$  is written within the quadratic approximation  $\gamma_\ell(\hat{\mathbf{k}}) = \gamma_0 + \gamma_2 \mathbf{k}^2$ , where the parameters  $\gamma_{0,2}$  are accessed from the condensate inhomogeneous spectral linewidth [24]. The interaction strength between polaritons is denoted by  $g$ , while  $g_R$  represents the interaction strength between the excitonic reservoir and polaritons. The complex noise  $\xi$  is Gaussian with zero mean  $\langle \xi \rangle = 0$  and a covariance  $\langle \xi(\mathbf{r}, t) \xi^*(\mathbf{r}', t') \rangle = 2\sigma \delta(\mathbf{r} - \mathbf{r}') \delta(t - t')$ . The amplitude  $\sigma$  originates from repeated gains from the reservoir and dissipation in the environment and reads  $\sigma = \frac{Rn_R + \gamma_0}{4}$  [19, 46].

When the external pump  $P$  is spatially homogeneous, exciton-polaritons undergo a condensation transition when  $P \geq P_{\text{th}} = \gamma_0 \gamma_R / R$ . Above this threshold, the condensate density  $|\psi|^2$  is non-zero and is given at the mean-field level by  $n_0 = \frac{\gamma_R}{R}(p-1)$  where  $p = P/P_{\text{th}}$ . Similarly, the mean-field excitonic density reads  $n_{R0} = \gamma_0 / R$ .

### III. UNIVERSAL REGIMES

#### A. KPZ effective dynamics

It is now well established that the dynamics of the phase of the driven-dissipative condensate maps under some conditions onto the KPZ equation [7, 18]. This is shown by writing the condensate wavefunction  $\psi$  in density phase representation  $\psi(\mathbf{r}, t) = \sqrt{n(\mathbf{r}, t)} e^{i\theta(\mathbf{r}, t) - i\Omega_0 t}$  with  $\Omega_0 = gn_0 + 2g_R n_{R0}$  and assuming scale separation between the spatio-temporal evolution of the density and the one of the phase [24]. Specifically, one assumes the condensate density to be stationary and smooth enough, so that  $\partial_t n \approx 0$  and  $|\nabla n| \approx 0$ . Further considering that the exciton reservoir density evolves adiabatically with respect to the condensate, one finds that the effective dynamics of the phase is governed by the KPZ equation [11]

$$\partial_t \theta = \nu \nabla^2 \theta + \frac{\lambda}{2} (\nabla \theta)^2 + \sqrt{D} \eta, \quad (3)$$

where  $\eta$  is a real Gaussian noise of zero mean  $\langle \eta \rangle = 0$  and delta-correlated in space and time  $\langle \eta(\mathbf{r}, t) \eta(\mathbf{r}', t') \rangle = 2\delta(\mathbf{r} - \mathbf{r}') \delta(t - t')$ . The KPZ effective parameters are given

in terms of the microscopic parameters by

$$\nu = \frac{\gamma_2}{2} + \frac{\hbar g_e}{2m g_i} \quad (4)$$

$$\lambda = -\frac{\hbar}{m} + \gamma_2 \frac{g_e}{g_i} \quad (5)$$

$$D = \frac{\sigma}{2n_0} \left[ 1 + \left( \frac{g_e}{g_i} \right)^2 \right], \quad (6)$$

where the effective polariton-polariton interaction strength under the adiabatic approximation is denoted  $g_e = g - 4 \frac{g_R g_i}{R}$  and with the losses  $g_i = \gamma_0^2 / 2P$ . In addition, the KPZ equation (3) can be rescaled to a unique nonlinearity parameter  $g_{\text{KPZ}} = \lambda^2 D / \nu^3$ .

The above mapping establishes a connection between the effective dynamics of a phase  $\theta(\mathbf{r}, t)$  and that of a classical interface of height  $h(\mathbf{r}, t)$  stochastically growing in the normal direction to the two-dimensional plane  $\mathbf{r}$ . This interface roughens in space and time and is characterized by a dynamical exponent  $z$ , a roughness exponent  $\alpha$ , a growth exponent  $\beta = \alpha/z$ , related in all dimensions by the exact identity  $\alpha + z = 2$ , stemming from the invariance of the KPZ equation (3) under an infinitesimal tilt of the interface [48]. In 1d, the values of the KPZ critical exponents are exactly known  $\alpha = 3/2$ ,  $z = 1/2$ ,  $\beta = 1/3$ . In 2d, no exact result is available but they have been determined through extensive numerical simulations of systems belonging to it, giving the estimates  $\alpha \approx 0.39$ ,  $z \approx 1.61$ ,  $\beta \approx 0.24$  [49–57].

The interface kinetic roughening is further characterized by its two-point correlation function  $C_{hh}(r, t) = \langle [h(\mathbf{r}, t) - h(\mathbf{0}, 0)]^2 \rangle$ , known to take the scaling form

$$C_{hh}(r, t) = C_0 t^{2\beta} F\left(y_0 \frac{r}{t^{1/z}}\right), \quad (7)$$

where  $C_0$ ,  $y_0$  are non-universal constants, and  $F(y)$  is the KPZ universal scaling function, calculated in 2d using functional renormalization group [58]. This function has the following asymptotics  $F(y) \xrightarrow{y \rightarrow 0} F_0$  finite and  $F(y) \xrightarrow{y \rightarrow +\infty} F_\infty |y|^{2\alpha}$  such that the correlation function behaves as a power-law both at coinciding space points  $C_{hh}(0, t) \sim t^{2\beta}$  and equal times  $C_{hh}(r, 0) \sim |r|^{2\alpha}$ .

Beyond its correlation properties, the universal features of the 2d growing interface can be classified to a greater extent from the distribution of its fluctuations, which indicates the existence of universality subclasses [59–62]. These subclasses are similar to the ones demonstrated for 1d interfaces in Refs. [12, 13, 63]. They correspond to different global geometries of the growth: flat, curved or stationary. They are associated with different probability distributions although sharing the same set of critical exponents. In contrast with the 1d case, where the form of these distributions is known exactly, being respectively the Tracy-Widom GOE, Tracy-Widom GUE, and Baik-Rains for these three subclasses [12, 13, 63], there is no analytical form for the 2d distributions.

## B. Weakly nonlinear EW regime

The Edwards-Wilkinson equation corresponds to the linear limit of the KPZ equation (3), *i.e.*  $\lambda = 0$  [2], from which the EW universality class is defined. Owing from its linearity, the properties of this equation can easily be worked out, and one can obtain in generic spatial dimension  $d$  the critical exponents  $\alpha_{\text{EW}} = \frac{2-d}{2}$ ,  $z_{\text{EW}} = 2$ ,  $\beta_{\text{EW}} = \frac{2-d}{4}$  as well as its correlation functions [44].

In both one and two dimensions, the EW fixed point of Eq. (3) is IR unstable when the nonlinearity  $g_{\text{KPZ}}$  is non-zero, and the renormalization group flow eventually reaches the KPZ fixed point. This means that the 2d interface always roughens. As a consequence, when  $\lambda \ll 1$ , the scaling behavior of  $C_{hh}(r, t)$  can be compatible with EW properties at small scales and at the early stages of the growth, but displays KPZ properties beyond some spatiotemporal scale which depends on  $1/g_{\text{KPZ}}$  [44]. This scenario was confirmed from numerical simulations of lattice models of interface growth, from the gradual change of the exponents with the nonlinearity parameter [55]. Finite-size effects have also been investigated for interfaces within the EW universality class, and for the crossover between the EW and the KPZ class [55, 64, 65].

The EW universality class is also relevant in the context of the complex Ginzburg-Landau equation (CGLE). While this deterministic equation is known to host a wide variety of patterned structures such as spirals, vortex glasses, as well as spatiotemporal chaos [66, 67], it also exhibits a regime, called phase turbulence, where the phase dynamics can be mapped into the Kuramoto-Sivashinsky equation [3, 4]. This deterministic equation has unstable modes which leads to chaos, such that its effective large-distance properties are known to belong to the KPZ universality class [68, 69]. However, in practice, huge system sizes and simulation times are required to actually observe the KPZ behavior, and otherwise the physical properties of the system display the EW universal features [70–73].

## C. Defects-dominated regime

A major difference between the usual KPZ equation [11] and the one obtained in Eq. (3) lies in the compactness of the phase  $\theta(\mathbf{r}, t)$ , which is defined on the support  $[-\pi, \pi[$ , whereas the interface  $h(\mathbf{r}, t)$  grows unbounded in  $\mathbb{R}$ . This specific feature has deep consequences on the growth of the phase interface  $\theta(\mathbf{r}, t)$ , as it renders possible the formation and proliferation of topological defects. Their nucleation has been studied building a dual electrodynamics theory for the compact version of the KPZ equation [30], and it was shown from a perturbative treatment in the nonlinearity  $\lambda$  that vortex-antivortex pairs should undergo a binding-unbinding mechanism, separating an algebraic quasi-ordered phase from a disordered one [31, 38]. This mechanism is characterized by a lengthscale  $L_v$  representing the typical defect interdis-

tance, that depends on the effective parameters  $\nu$ ,  $\lambda$  and  $D$  of the KPZ equation. Numerical simulations of the compact KPZ equation indicate that defect nucleation is hindered for systems smaller than  $L_v$  [39].

The deterministic part of the gGPE (1) describing the condensate dynamics is well approximated by the 2d CGLE. At variance with the vortices in the compact version of the KPZ equation, the phase defects of the CGLE are pinned to density holes, that are continuously replenished by the external drive. This causes an outward polariton flow from these holes, which in return dramatically affects the interaction between vortex pairs [32, 33], creating notably self-accelerated motion of the vortex cores [32, 74].

However, the stochastic part of the gGPE (1) is known to modify the phase diagram of the 2d CGLE, *e.g.* destroying vortex glasses, affecting the motion of spiral vortices, and creating additional free vortices [67, 75]. It was also pointed out that phase defects can appear in the space-time map of the phase [25]. These space-time vortices are noise-activated, and their density was found to be proportional to  $e^{-\frac{p-1}{\sigma}}$  in 1d [26]. While KPZ universal features were shown to be robust to small defect densities in both 1d and 2d condensates [24, 26, 76], they are superseded by new properties in the vortex dominated phase.

## IV. RESULTS

### A. Numerical simulations

We solve numerically the gGPE (1) with periodic boundary conditions by propagating the initial condition in time with a symmetrized split-step method [77]. We implement the stochastic part of the dynamics by adding to the wave function  $\psi(\mathbf{r}, t)$ , at each time step and for each spatial point, a complex random number generated by a Euler-Maruyama algorithm, reproducing the statistical properties of the Gaussian noise  $\xi$ . We solve the reservoir dynamics (2) by using a first order Euler scheme.

The parameters of the simulation are chosen to reproduce typical experimental conditions in GaAs microcavities [24]:  $\hbar\gamma_0 = 197.5\mu\text{eV}$ ,  $\hbar\gamma_2 = 1.77 \times 10^4\mu\text{eV}\cdot\mu\text{m}^2$ ,  $\gamma_R = 0.45\gamma_0$ ,  $R = 57.3 \times 10^{-3}\mu\text{m}\cdot\text{ps}^{-1}$ ,  $P = 2P_{\text{th}}$ . The polariton-polariton interaction strength  $g$  is set to zero, and the interaction between the exciton reservoir and polaritons  $g_R$  is chosen from the value of the blueshift at threshold  $\mu_{\text{th}}$  and the steady-state reservoir density,  $g_R = \frac{1}{2}\mu_{\text{th}}/n_{R0}$ . The blueshift at threshold  $\mu_{\text{th}}$  is varied from  $50\mu\text{eV}$  to  $700\mu\text{eV}$  in order to access the different universal regimes presented in Sec. III. The polariton mass is chosen negative  $m = -4 \times 10^{-5}m_e$  so as to counterbalance the sign of the effective interactions ( $g_e < 0$ ) and preserve the condensate stability [42]. The noise amplitude is approximated in the following by  $\sigma \approx Rn_R/2$ .

We perform the numerical simulations on a square lattice of spacing  $\ell = 2.83\mu\text{m}$  to mimic the structure of a square lattice of  $N \times N$  optical micropillars, and the number of sites is  $N = 64$  (unless otherwise mentioned). The integration time-step  $dt$  is varied linearly with the blueshift at threshold  $\mu_{\text{th}}$  from  $3 \times 10^{-2}\text{ps}$  to  $8 \times 10^{-3}\text{ps}$ , such that the phase dynamics remains well resolved in time. The solution of the stochastic condensate dynamics Eq. (1) reaches a steady state at a time  $t_0$  which depends on the chosen microscopic parameters. In the steady state, the spatially averaged density is stationary. In the remainder of this article, we focus on the steady-state properties of the condensate for times larger than  $t_0$ .

### B. Identification of the three regimes

In the following, we show that the three regimes presented in Sec. III are accessible by tuning the nonlinear parameter  $g_{\text{KPZ}} = \frac{\lambda^2 D}{\nu^3}$ , whose dependence on the microscopic parameters is known from Eqs. (4)–(6). This effective nonlinearity can be tuned over a broad range of values by changing the blueshift at threshold  $\mu_{\text{th}}$ , which controls the effective polariton interaction strength  $g_e$ . It can be modified through the excitonic fraction in the polaritonic state [43], and it thus provides a natural candidate to explore the universal properties of the 2d condensate.

We solve the condensate dynamics Eqs. (1)–(2) for many values of  $\mu_{\text{th}}$ , and indeed identify three distinct regimes, which correspond to the EW, the KPZ and the vortex regimes of Sec. III. We first provide a qualitative picture, by displaying in Fig. 1 typical density and phase maps, which are snapshots at an arbitrary instant in the steady state, for each of these regimes. The density (left column) appears almost identical in both the EW (upper row) and the KPZ (middle row) regimes. In the vortex phase (bottom row), the condensate density visibly spreads out toward lower values, and interacting vortices are discernible. Regarding the phase (right column), a clear difference is however noticeable between the EW and KPZ regimes from the spread of the phase values. In the vortex regime, the phase explores entirely its compact support and phase defects are visible at spatial points mixing all the colors together, and coinciding with holes in the density map, indicating a strong correlation between the density and phase fields.

### C. Steady-state condensate density

We compute for a wide range of interaction strength the steady state density, averaged over space and noise realizations. Simulations are performed over  $10^6\text{ps}$  to let the condensate relax to its steady state, and the numerical convergence is sped up by sampling each initial

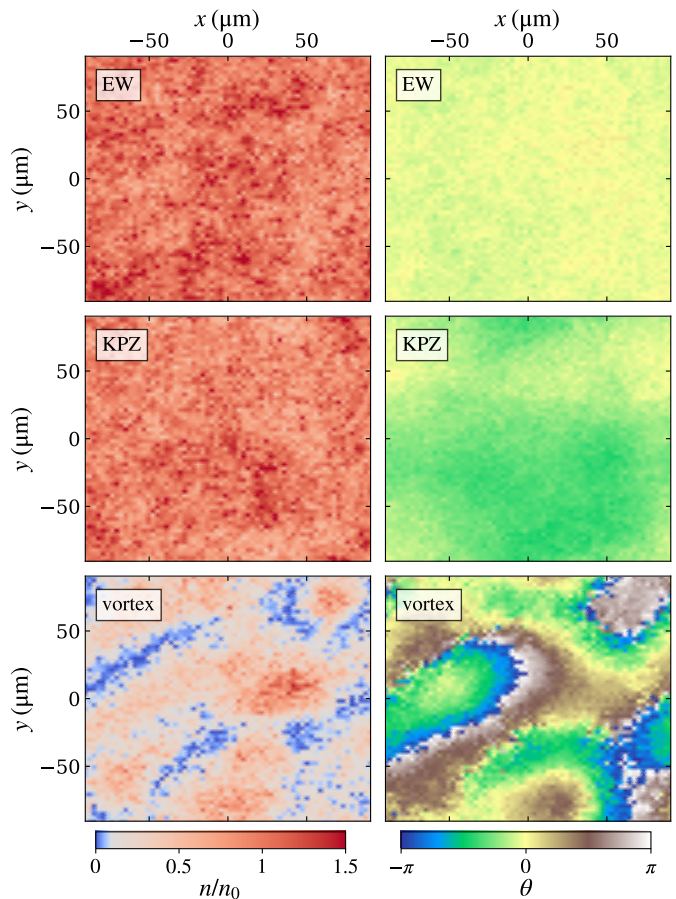


FIG. 1. Typical stationary density (left column) and phase (right column) maps, for an arbitrary time instant in the steady-state, in the three different universal regimes: (EW)  $\mu_{\text{th}} = 50\mu\text{eV}$ , (KPZ)  $\mu_{\text{th}} = 429\mu\text{eV}$ , (vortex)  $\mu_{\text{th}} = 700\mu\text{eV}$ . The condensate density  $n(x, y)$  is normalized by its mean field value  $n_0$ .

condition from the steady state configuration reached by the condensate for the previous value of  $\mu_{\text{th}}$ .

Results are shown as a function of the blueshift at threshold on the upper panel of Fig. 2, revealing a sharp transition at  $\mu_{\text{th}} \approx 480\mu\text{eV}$ . This abrupt drop of density is related to the transition from a vortex-free condensate with very few space-time vortices to a defect-dominated phase (blue-shaded area). A similar transition was reported in Ref. [35] as a result of modulational instability [26, 42, 78, 79], whereas in the present case it rather seems to be related to the competition between the finite system size and the typical vortex separation  $L_v$  scale [39], establishing a transition from a phase turbulent to a defect turbulent regime [70].

The precise location of the transition point is blurred out due to finite-size effects, and to the fact that we observe extended relaxation timescales in the presence of vortices, which are consistent with the ones reported in Ref. [40]. The slow relaxation induced by the presence of vortices was also noted in the relaxation dynamics of the

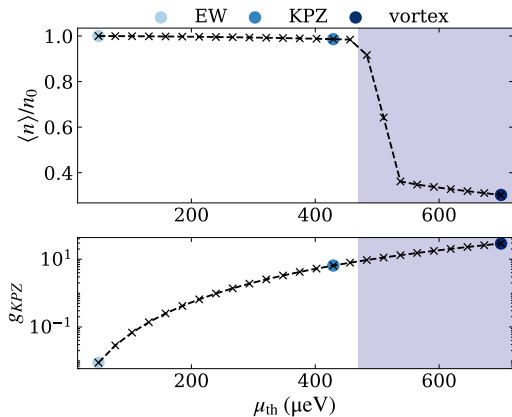


FIG. 2. Condensate density averaged over space and 128 realizations of the noise, normalized by  $n_0$  (upper panel) and effective KPZ nonlinearity defined from Eq. (3) (lower panel) as a function of the blueshift at threshold  $\mu_{th}$ . Light, medium, and dark blue circles indicate points of the phase diagram corresponding to the EW, KPZ, and vortex regime respectively.

equilibrium XY model [80]. Thus, in order to confirm the position of the defect phase indicated by the blue-shaded area, we ran the algorithm from both sides, *i.e.* for both increasing and decreasing  $\mu_{th}$ .

We also show on Fig. 2 (lower panel) the corresponding values of the effective KPZ non-linearity  $g_{KPZ}$ . EW properties are expected to be dominant in the weakly nonlinear regime reached for small  $\mu_{th}$ , followed by KPZ properties at intermediate  $\mu_{th}$ , before the vortex-dominated phase sets in. Three points representative of these three regimes are indicated on Fig. 2. They correspond to the three values chosen for the maps of Fig. 1.

In the following, we characterize the properties of these three regimes through their first-order coherence, their momentum distribution, and their fluctuations statistics.

#### D. First-order correlation $g^{(1)}(r, t)$

Each of the regimes presented in Sec. III deeply imprint the phase dynamics of the EP condensate, and therefore its coherence properties. They can be distinguished experimentally in the spatiotemporal decay of the condensate first-order correlation function, defined as

$$g_{\psi}^{(1)}(\Delta r, \Delta t) = \frac{\langle \psi^*(\Delta \mathbf{r} + \mathbf{r}_0, \Delta t + t_0) \psi(\mathbf{r}_0, t_0) \rangle}{\sqrt{\langle n(\Delta \mathbf{r} + \mathbf{r}_0, \Delta t + t_0) \rangle \langle n(\mathbf{r}_0, t_0) \rangle}} \quad (8)$$

where the average  $\langle \cdot \rangle$  is performed over realizations of the stochastic dynamics (1) in the steady state, as well as over the circle of radius  $\Delta r = |\Delta \mathbf{r}|$  exploiting isotropy. This correlation function encompasses contributions from both the density and the phase, and approximately reads

$$g_{\psi}^{(1)}(\Delta r, \Delta t) \approx g_n^{(1)}(\Delta r, \Delta t) \langle e^{i[\theta(\Delta \mathbf{r} + \mathbf{r}_0, \Delta t + t_0) - \theta(\mathbf{r}_0, t_0)]} \rangle \quad (9)$$

when density-phase correlations are negligible, with

$$g_n^{(1)}(\Delta r, \Delta t) = \frac{\langle \sqrt{n(\Delta \mathbf{r} + \mathbf{r}_0, \Delta t + t_0) n(\mathbf{r}_0, t_0)} \rangle}{\sqrt{\langle n(\Delta \mathbf{r} + \mathbf{r}_0, \Delta t + t_0) \rangle \langle n(\mathbf{r}_0, t_0) \rangle}}. \quad (10)$$

This is the case both in the EW and in the KPZ regimes. Additionally assuming that density-density correlations are negligible  $g_n^{(1)}(\Delta r, \Delta t) \approx 1$  and performing a cumulant expansion of the phase term one obtains [24]

$$-2 \log \left[ |g_{\psi}^{(1)}(\Delta r, \Delta t)| \right] \simeq C_{\theta\theta}(\Delta r, \Delta t) \quad (11)$$

where  $C_{\theta\theta}(\Delta r, \Delta t)$  is the connected two-point correlation function of the phase defined as for the KPZ height-height correlator Eq. (7). In the following we adopt the short-hand notation  $\mathcal{G}_{\psi, n}^{(1)}(\Delta r, \Delta t) \equiv -2 \log \left[ |g_{\psi, n}^{(1)}(\Delta r, \Delta t)| \right]$ .

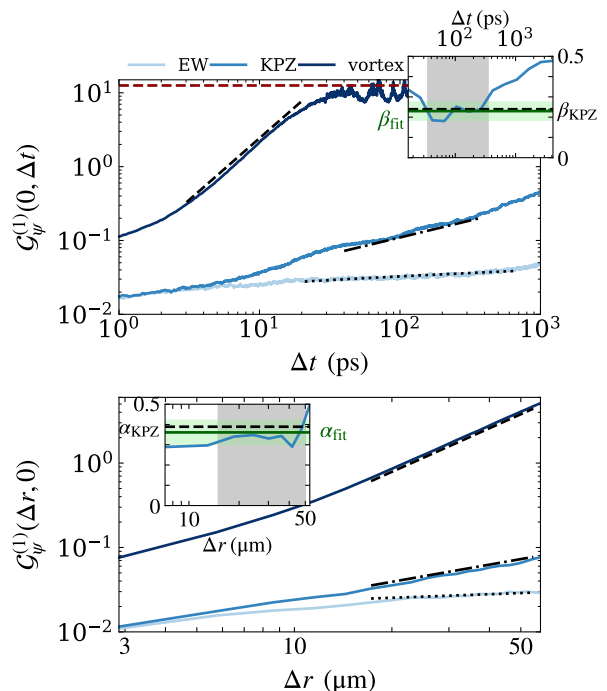


FIG. 3. Equal-space (upper panel) and equal-time (lower panel) first-order correlation function corresponding to the EW, KPZ, and vortex points of Fig. 2. A logarithmic fit is plotted in dotted line for the former, and guidelines are shown in dash-dotted and dashed line for the two latter. The red horizontal dashed line corresponds to the expected saturation value of  $g^{(1)}(0, \Delta t)$  in the absence of density correlations and for  $\text{Var}[\theta(\mathbf{r}_0, \Delta t + t_0) - \theta(\mathbf{r}_0, t_0)] = 2\pi$ . The local exponents, computed according to Eqs. (14a)–(14b), are shown for the KPZ point in the insets, where the grey shade extends, as the dash-dotted line, over [35ps, 350ps] and [15μm, 50μm] respectively.

It follows from the mapping (3) and (11) that if the phase of the condensate obeys at some spatiotemporal



scales a KPZ dynamics, the coherence of the condensate endows the scaling form

$$\mathcal{G}^{(1)}(\Delta r, \Delta t) \sim \begin{cases} \Delta t^{2\beta_{\text{KPZ}}}, & \Delta r = 0 \\ \Delta r^{2\alpha_{\text{KPZ}}}, & \Delta t = 0 \end{cases}, \quad (12)$$

as suggested in early studies of the CGLE [71]. As already mentioned in Sec. I, this behavior has been confirmed in experimental realizations of 1d polariton condensates [24], as well as in numerical simulations of their 2d analog [8, 76].

For weak but non-vanishing nonlinearity, EW correlations are expected to persist for extended scales before KPZ features arise. While stretched exponential decays of  $g^{(1)}$  are expected in 1d in the EW phase as in the KPZ phase [9], the situation changes in 2d as a result of the vanishing of  $\alpha_{\text{EW}}$  and  $\beta_{\text{EW}}$  (Sec. III B). This yields instead logarithmic growth as predicted from the solution of the EW equation [44]

$$\mathcal{G}^{(1)}(\Delta r, \Delta t) \sim \begin{cases} \frac{D}{2\pi\nu} \ln(\Delta t \Lambda^2), & \Delta r = 0 \\ \frac{D}{\pi\nu} \ln(\Delta r \Lambda), & \Delta t = 0 \end{cases}, \quad (13)$$

with  $\Lambda$  a UV cutoff. This implies an algebraic decay of  $g^{(1)}$  in space as  $g^{(1)}(\Delta r, 0) \sim \Delta r^{-a_s}$  with exponent  $a_s = D/2\pi\nu$ , and in time as  $g^{(1)}(0, \Delta t) \sim \Delta t^{-a_t}$  with exponent  $a_t = D/4\pi\nu$ . Such a behavior was predicted within Bogoliubov theory [81, 82] and observed in experiments [83] but however never related to EW universal features. This identification, motivated by the mapping (3) as well as results shown on Fig. 2, appears crucial in guiding the observation of KPZ universality in 2d polariton condensates. Moreover, this result provides a quantitative explanation for the exponent ratio estimated numerically as  $a_s \simeq 2a_t$  [34], as well as for the recent experimental observation [84] that  $a_s \propto 1/n_0$  from which it was suggested  $a_s \propto \frac{\sigma/n_0}{\hbar/m}$  in analogy with equilibrium condensates. Indeed, (13) captures this behavior through  $a_s \propto \frac{D}{\nu}$ , where the nonequilibrium nature of the polariton condensate appears explicitly in the effective noise (6) and viscosity (4) of the phase. The general correspondence between Bogoliubov prediction for the large space and time behavior of the phase correlation and EW properties is detailed in Appendix A.

The first-order correlation function is computed in the steady state of the condensate according to Eq. (8), and averaged over 1024 realizations of the noise. The results obtained in the three regimes are shown on Fig. 3. In the weak nonlinearity regime (light blue), algebraic decays consistent with EW behavior (13) are observed, and the corresponding fits are shown as dotted line, where we find  $a_s/a_t = 1.8 \pm 0.1$ . These fits are performed in a restricted spatiotemporal window (grey-shaded area). Its lower bound corresponds to the time where density correlations, displayed in Fig. 4, are negligible ( $\mathcal{G}_n^{(1)}$  is flat) such that the first-order correlation function is fully determined by the phase. Its upper bound corresponds to

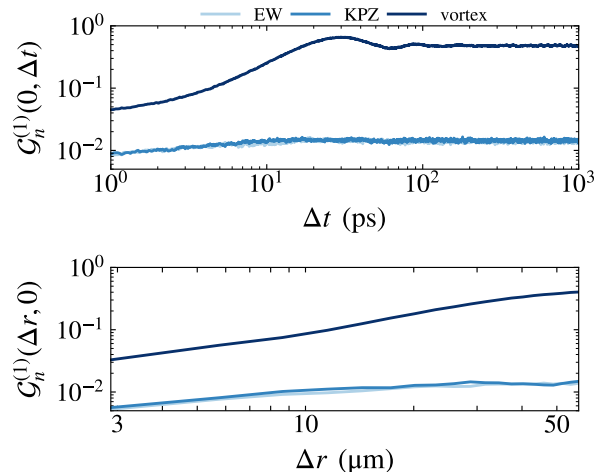


FIG. 4. Equal-space (upper panel) and equal-time (lower panel) second-order correlation function.

the time when  $g^{(1)}(0, \Delta t)$  develops an exponential decay induced by the finite system size (discussed in Sec. IV E).

At intermediate values of  $\mu_{\text{th}}$  (medium blue), a clear departure from EW behavior is observed. This departure is induced by phase correlations, as shown on Fig. 4, where the decay of density correlations perfectly matches the one at the EW point, indicating that approximations leading to the effective phase dynamics (3) are valid. Reservoir effects are visible at times  $\Delta t \approx 10$  to 30ps and naturally arise when interactions are increased or for high values of the pumping rate [26, 76]. Proceeding as in Ref. [76], we compute the local exponents according to

$$\alpha \approx \frac{1}{2} \frac{d}{d \ln(\Delta r)} \ln \left[ \mathcal{G}^{(1)}(\Delta r, 0) \right] \quad (14a)$$

$$\beta \approx \frac{1}{2} \frac{d}{d \ln(\Delta t)} \ln \left[ \mathcal{G}^{(1)}(0, \Delta t) \right]. \quad (14b)$$

Results are shown in the insets of Fig. 3. The exponents are extracted within the windows of interest, *i.e.* after density or reservoir effects and before finite size effects. We find  $\beta_{\text{fit}} = 0.23 \pm 0.04$  and  $\alpha_{\text{fit}} = 0.36 \pm 0.06$ , which are in good agreement with exponents obtained from numerical resolution of discrete models in the 2d KPZ universality class [51]. These fitted exponents are used to plot the dash-dotted guidelines on Fig. 3, in windows indicated as the grey shades over 315ps in time and 35 $\mu\text{m}$  in space.

At large values of  $\mu_{\text{th}}$  (dark blue), the first-order correlation function decays very rapidly in both space and time due to the proliferation of phase defects, and saturates in time to  $g^{(1)} \approx e^{-2\pi}$  when the compact phase completely spreads in  $[-\pi, \pi]$ . Stretched exponential decays of the form of (12) are indicated by dashed guidelines, with  $\alpha_v = 0.857 \pm 0.005$  and  $\beta_v = 0.835 \pm 0.003$ , which lie within the range of values reported in Ref. [29] while clear exponential decays ( $\alpha_v = \beta_v = 0.5$ ) were

found in Ref. [34]. It should also be noted that density correlations exhibit oscillations in time (upper panel Fig. 4), which are found independent on  $g_R$  but sensitive on the pumping rate  $p$ . This numerical observation could be of experimental relevance for the characterization of the defect regime, and calls for further theoretical investigations that go beyond the scope of this work.

### E. Finite-size effects

The spatio-temporal windows where EW or KPZ critical exponents can be measured are very small, which hinders the observability of these regimes. However, interestingly, these exponents also imprint the exponential decay superseding the EW-KPZ regimes, through finite-size effects. We thus now investigate this exponential decay, which can be observed on Fig. 3 in the equal-space first-order correlation function at the latest times. For this, we compute the condensate first-order correlation function averaged over 256 realizations of the noise at the EW point of Fig. 2 increasing the system size  $N \times N$  from  $N = 8$  to  $N = 256$  for temporal correlations and up to  $N = 1024$  for spatial correlations. Results are shown on Fig. 5, where one observes that the condensate coherence preserves a quasi long-range order down to millimetre lengths. As a function of time, the condensate exhibits quasi long-range order up to a crossover time, that depends on the system size, from which the decay becomes exponential. This result can be summarized in the following scaling form for the equal-space phase-phase correlator

$$C_{\theta\theta}(0, t) \sim t^{2\beta} f\left(\frac{t}{L^z}\right), \quad (15)$$

which was first formulated in the context of kinetically roughening interfaces [85], then suggested in the context of the CGLE [71], and very recently again in the large time decoherence of 1d driven-dissipative condensates [86]. A derivation of Eq. (15) is presented within Bogoliubov theory in both one and two dimensions in Appendix A. This equation represents the change in behavior of correlations between their thermodynamics limit and their saturation to Brownian motion, when the growing interface (here the phase) loses the memory of its initial condition [85].

In 2d and in the weakly nonlinear regime where  $z = 2$ , one finds  $f(t/L^z) \underset{t \ll L^z}{\sim} \log(t/L^z)$  which reproduces the algebraic decay of the condensate coherence in Eq. (13). At large times  $t/L^z \gg 1$ ,  $f(y) \sim y^{1-2\beta}$ , from which we obtain  $g^{(1)}(0, \Delta t) \sim e^{-\Delta t/\tau_c}$  with the coherence time  $\tau_c \sim L^{z-2\alpha}$ . This means that while the condensate decoherence is constrained to an exponential decay at large times no matter  $z$  and  $\alpha$ , the coherence time keeps the memory of the underlying universality class through its dependence on the system size. This could be of great importance to identify KPZ universal features in 2d po-

lariton condensates given the limited extent of the temporal scaling in its one-dimensional experimental realization [24], and notably in our case due to finite size effects as seen on Fig. 3. In the weakly nonlinear limit

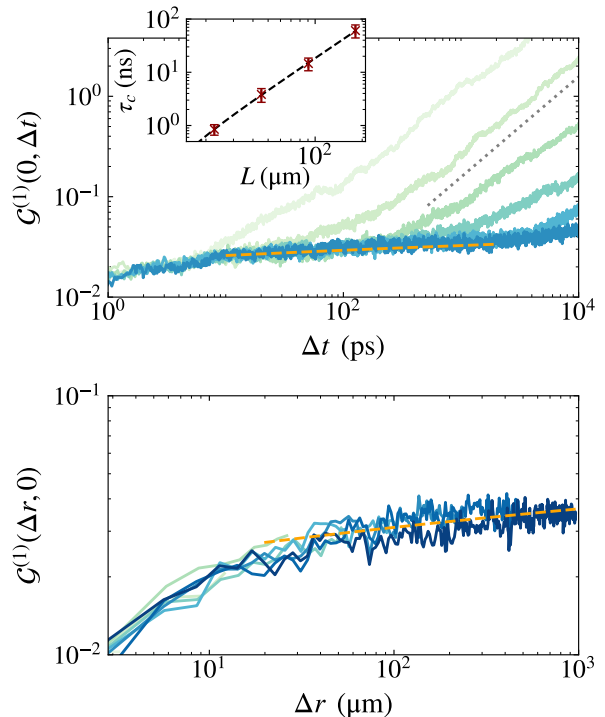


FIG. 5. First-order correlation function at the EW point of Fig. 2 for a system of  $N = 2^i$  linear sites, at (upper panel) equal-space with  $i = \{3, \dots, 8\}$ , and (lower panel) equal-time with  $i = \{3, \dots, 10\}$ . The colorscale is growing with the system size from light green to dark blue. Algebraic decays are represented by the fitted orange dashed line. A grey dotted line indicates the large time exponential decay. Inset: coherence time  $\tau_c$  fitted from the large-time exponential decay of  $g^{(1)}(0, \Delta t)$  as a function of the system size  $L$ .

under consideration here we expect  $\tau_c \sim L^2$ , which coincides with the Schawlow-Townes coherence time of 2d lasers [87, 88]. The coherence time  $\tau_c$  is extracted from the exponential decay of Fig. 5 and plotted in the inset. Fitting these values with a power law ansatz, we find  $\tau_c \sim L^{1.98 \pm 0.07}$  which is in perfect agreement with the expected EW scaling exponents.

When the nonlinearity  $\lambda$  is large enough to let KPZ features arise, we expect  $\tau_c \sim L^{0.83}$ . Proceeding in the same manner as above, we compute the condensate first-order correlation function averaged over 2048 realizations at the KPZ point of Fig. 2, varying  $N$ . As we have discussed in Sec. IV C, the position of the transition in Fig. 2 depends on the size of the system, causing the phase turbulence regime where KPZ features are observed to disappear in favour of defect turbulence if the system size is too large. For this reason,  $N$  is varied from 32 to 64 only. Results are shown on Fig. 6, where the spatial decoherence (lower panel) visibly converges to the KPZ scal-



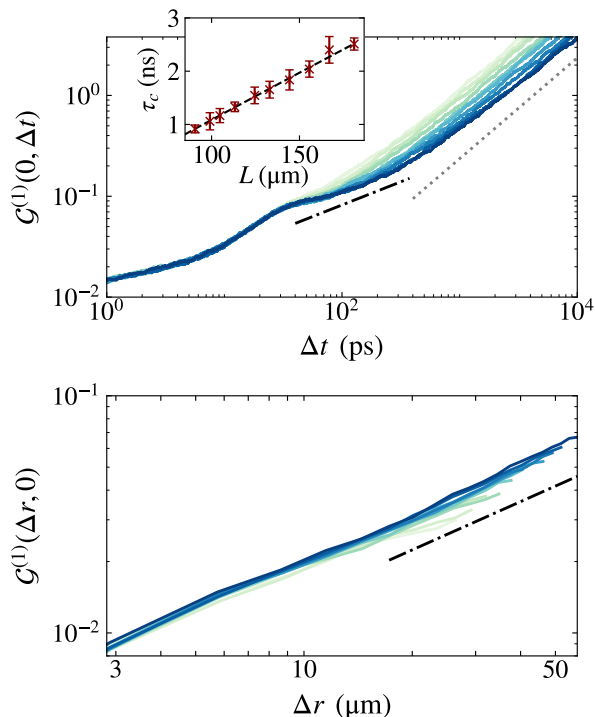


FIG. 6. First-order correlation function at the KPZ point of Fig. 2 for a system of  $N = 32$  to 64 linear sites, at (upper panel) equal-space, and (lower panel) equal-time. The colorscale is growing with the system size from light green to dark blue. Algebraic decays are represented by the dash-dotted line. A grey dotted line indicates the large time exponential decay. Inset: coherence time  $\tau_c$  fitted from the large-time exponential decay of  $g^{(1)}(0, \Delta t)$  as a function of the system size  $L$ .

ing as the system size increases, as observed in Ref. [8]. The temporal decoherence (upper panel) shows that KPZ features are dramatically affected when the system gets smaller, the scaling window becoming hardly discernible. However, its signature remains accessible from the coherence time according to Eq. (15), whose dependence on the system size is close to linear (Inset of Fig. 6) and clearly differs from the parabola obtained on Fig. 5. Fitting the numerical values of the coherence time with a power law ansatz, we find  $\tau_c \sim L^{0.97 \pm 0.18}$ , which closely encloses the prediction from KPZ exponents and discard the one from EW exponents.

### F. Momentum distribution $n_{\hat{k}}$

We now compute the momentum distribution of the condensate, defined as

$$n_{\hat{k}} = \langle \psi^*(\hat{\mathbf{k}}, t_0) \psi(\hat{\mathbf{k}}, t_0) \rangle, \quad (16)$$

where  $\psi(\hat{\mathbf{k}}, t_0)$  is the Fourier transform of the condensate wave function. The results are displayed on Fig. 7 for

the three points shown on Fig. 2. Let us first comment on the behavior of the momentum distribution for the large values of  $k$ . In the adiabatic approximation of the reservoir, Bogoliubov theory predicts in the continuous limit that the momentum distribution is determined by the microscopic properties of the condensate according to  $n_{\hat{k}} \propto \sigma / \gamma_2 k^2$  (see Appendix A). We therefore expect the three curves to share the same decay at large  $k$ . This is indeed observed, and the momentum distribution decays as  $n_{\hat{k}} \sim k^{-1.893 \pm 0.004}$ , represented on Fig. 7 by a dashed guideline, in good agreement with the theoretical prediction.

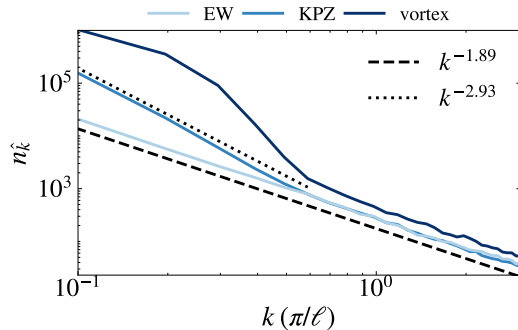


FIG. 7. Momentum distributions corresponding to the EW, KPZ, and vortex points of Fig. 2 and averaged over 256 realizations of the noise. Dashed and dotted guidelines indicate the power laws  $k^{-1.893 \pm 0.004}$  and  $k^{-2.93 \pm 0.03}$  respectively.

At small momenta, we expect  $n_{\hat{k}}$  to depend on the condensate macroscopic properties, so that it should behave differently in the three regimes under consideration. Within the conditions of validity of Bogoliubov theory, in particular for small density fluctuations, we find  $n_{\hat{k}} \propto D / \nu k^{2\beta z + 2}$ . This leads to the prediction  $n_{\hat{k}} \propto D / \nu k^2$  at the EW point. On Fig. 7, we rather observe  $n_{\hat{k}} \sim k^{-1.893 \pm 0.004}$  as in the large  $k$  regime, which is in good agreement with the theoretical expectation. At the KPZ point, nonlinearity comes into play and the scaling is expected to change to  $n_{\hat{k}} \sim k^{-2.77}$ . The observed behavior is fairly close to this prediction, as we obtain  $n_{\hat{k}} \sim k^{-2.93 \pm 0.03}$  as shown by the dotted guideline.

In the vortex phase, density fluctuations are large and the momentum distribution is expected to display structures that depend on both the typical vortex radius and their average interdistance. The curve shown on Fig. 7 displays such a structure, which appears similar to the one observed in the soliton phase of 1d condensates [26].

### G. Distribution of condensate phase and density fluctuations

In this section, we compute the probability distributions of the fluctuations of the phase and of the density in the stationary state for the three regimes highlighted

on Fig. 2. Let us start with the phase. As already mentioned in Sec. III A, interfaces in the KPZ universality class exhibit universal probability distributions of their fluctuations belonging to three main subclasses. This is encapsulated in the following asymptotic relation

$$h(\mathbf{r}_0, t) \underset{t \rightarrow +\infty}{\sim} v_\infty t + (\Gamma t)^{\beta_{\text{KPZ}}} \chi(\mathbf{r}_0, t), \quad (17)$$

where the first term describes the deterministic growth of the interface, and where  $v_\infty$  and  $\Gamma$  are two non-universal constants whose exact expression depends on the underlying microscopic model [89]. The second term in Eq. (17) encompasses the fluctuations, which grow in time with the KPZ scaling, and where  $\chi$  is a random variable. Its probability distribution depends on the geometry of the growing interface, distinguishing three universality subclasses that correspond to flat, curved or stationary geometries. Each of them possesses a finite skewness and kurtosis, signaling a clear departure from the EW linear theory ( $\lambda = 0$ ) which is characterized by Gaussian fluctuations. These subclasses can be probed, in practice, through the distribution of reduced height fluctuations defined as  $\tilde{h} = [\Delta h(\Delta t + t_0) - \Delta h(t_0)] / (\Gamma \Delta t)^{\beta_{\text{KPZ}}}$ , with  $\Delta h = h - \langle h \rangle$  at a fixed space point  $\mathbf{r}_0$ . For 1d interfaces, these probability distributions are given by Tracy-Widom GOE, Tracy-Widom GUE, and Baik-Rains distributions respectively [12, 63]. This was extensively confirmed for interfaces from both numerical [90, 91] and experimental studies [92–95]. These three universality subclasses were also realized for the phase of 1d polariton condensates, adding an external confining potential to induce a geometric constraint on the phase of the condensate [22, 23].

The same asymptotic form Eq. (17) holds in 2d, where three subclasses have also been identified in numerical simulations of models belonging to the 2d KPZ universality class. There are no known analytical forms for the corresponding distributions, and only empirical fitting functions are available. For the 2d analogs of the flat and curve interfaces, a generalized Gumbel distribution of parameter  $m = 6$  and 9.5 respectively has been proposed [59, 61, 62], and for the stationary geometry a Pearson type IV distribution [60]. This seemed to be confirmed by experiments although 2d growing interfaces are not fully controlled [96–98], and two of the three subclasses have been reported in the phase of 2d EP BECs [23, 40].

To confirm the scaling observed on Fig. (3) at the KPZ point of Fig. (2), we record 5120 realizations of the condensate dynamics from which we extract phase trajectories in time in the steady state and unwrap them in  $\mathbb{R}$  for a given spatial point. The presence of defects creates time-resolved  $2\pi$  jumps in the unwrapped phase, creating secondary peaks in the distribution of fluctuations [24, 76]. However, very few phase jumps occur even for large times for the parameters corresponding to the KPZ regime, so that the unwrapped phase can safely be considered as a continuous interface in the temporal window

of interest. Typical trajectories are shown on Fig. 8. The

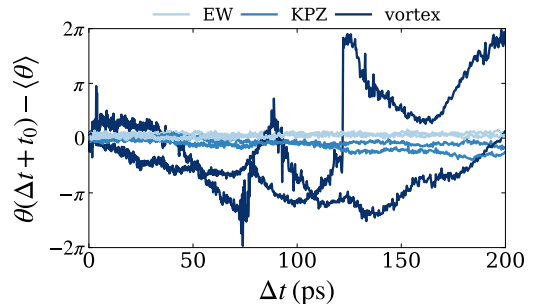


FIG. 8. Two typical unwrapped phase trajectories for each of the three regimes corresponding to the EW, KPZ, and vortex points of Fig. 2 (with the same color code). A  $2\pi$  phase jump is visible on one of the vortex phase trajectories.

normalized probability distribution of reduced phase fluctuations  $\tilde{\theta}$ , defined by

$$\tilde{\theta}(\Delta t, t_0) = \text{sign}(\lambda) \frac{\Delta\theta(\Delta t + t_0) - \Delta\theta(t_0)}{\text{Var}[\Delta\theta(\Delta t + t_0) - \Delta\theta(t_0)]} \quad (18)$$

where  $\Delta t \in [35\text{ps}, 350\text{ps}]$  as shown on Fig. 3, is displayed on Fig. 9. The  $\text{sign}(\lambda)$  in (18) stems for the negative value obtained for  $\lambda$  with our parameters, which flips the distribution into its mirror image compared with the theoretical predictions obtained for  $\lambda > 0$  [22, 24]. The distribution of phase fluctuations exhibits clear non-Gaussian tails. As  $\Delta t/t_0 \sim 0.1$  in our simulations, we expect it to be described by the Pearson distribution. The latter is represented with a dashed blue line together with our numerical data on Fig. 9, showing a perfect agreement with the expected KPZ distribution.

Proceeding in the same way for the EW point of Fig. 2 we obtain a Gaussian distribution instead (light blue histogram on Fig. 9), clearly confirming the slow crossover between an EW phase and the KPZ phase presented earlier. Typical unwrapped phase trajectories at the EW point are shown on Fig. 8. Let us note that this result is in agreement with the one found in numerical simulations of the deterministic 2d CGLE [70], where only the EW could be observed since in the deterministic case, tremendously large spatiotemporal scales are needed for KPZ features to arise [99].

Following the same method for the vortex point of Fig. 2, we compute the probability distribution of unwrapped phase fluctuations in the time window where the first-order correlation function is saturated. At this point, phase trajectories behave erratically and numerous defects are visible in Fig. 8. We obtain an histogram for  $\tilde{\theta}$  compatible with a double exponential distribution (dark blue squares on Fig. 9). This indicates that phase jumps occur independently and at a constant rate in time, as was suggested in Refs. [25, 26]. This can be modeled by a Laplace distribution  $\propto e^{-|\tilde{\theta}|/b}$ , where we find  $b \simeq 0.7$  from the fit of the numerical data.

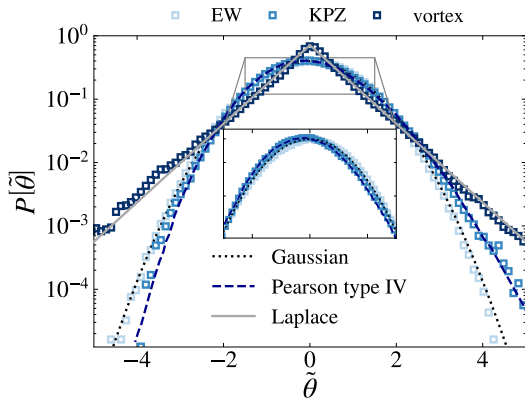


FIG. 9. Centered and rescaled distributions of phase fluctuation  $\tilde{\theta}$  corresponding to the EW, KPZ, and vortex points of Fig. 2. The two former histograms are composed of approximately  $1.5 \times 10^6$  data, and approximately  $7 \times 10^6$  for the latter. The centered and unit-variance 2d stationary KPZ distribution [60] is shown by a dark blue dashed line, together with a centered and unit-variance Gaussian distribution. The grey plane line is a centered Laplace distribution of parameter  $b = 0.7$ .

We now turn to the study of density fluctuations. We extract for each of the three regimes shown on Fig. 2 the density fluctuations in the stationary regime from 128 independently produced spatial maps. Results are shown on Fig. 10, where we have normalized the density by its mean-field value  $n_0$  for convenience. First we observe

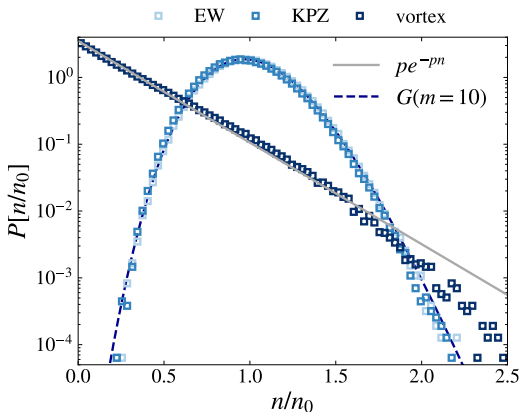


FIG. 10. Histograms of the density  $n$  normalized by its mean-field value  $n_0$  corresponding to the EW, KPZ, and vortex points of Fig. 2. Each histogram contains approximately  $5 \times 10^5$  datas. The two formers are fitted by a Gumbel distribution of parameter  $m = 10$ , mean  $\langle n \rangle/n_0$ , and variance  $\text{Var}[n/n_0]$ , shown by the dashed blue line. The latter is fitted by an exponential distribution of parameter  $p = 3.5$ .

that the density distribution at the EW and at the KPZ point perfectly match, which is not too surprising from Figs. 2 and 4. However, unexpectedly, these distributions exhibit clear deviations from a Gaussian distribution and

have finite skewness and kurtosis. A possible origin could be a subleading coupling between density and phase, but a definite conclusion requires further studies which are beyond the scope of this work. We find that they are well fitted by a Gumbel distribution of parameter  $m = 10$ . At the vortex point, the density distribution markedly differs and is rather fitted by an exponential distribution. This indicates again that the formation of defects occurs randomly, following a Poisson process. Similar exponential distributions have been reported in the nucleation time distribution of spiral defects, in the context of the 2d CGLE [100], and the discrepancies on Fig. 10 between the histogram and the exponential distribution at large  $n/n_0$  can be explained by finite size effects [70].

## V. CONCLUSION

In this paper, through extensive numerical simulations of a generalized Gross-Pitaevskii equation, we have explored the universal properties of a 2d exciton-polariton condensate under incoherent pumping. Controlling the effective nonlinearity of the phase dynamics through the interaction strength between reservoir excitons and polaritons, we have identified three different regimes: a first one for small nonlinearity where the dynamics of the density and of the phase are decoupled, and where the phase exhibits EW universal properties, a second one at intermediate nonlinearity where the density and phase are still decoupled but where the phase roughens with properties belonging to the KPZ universality class, a third one for large values of the nonlinear parameter, where density and phase fluctuations are coupled, since spatial vortices induce both phase singularities and deep minima in the condensate density at the positions of the vortex cores.

We have characterized the properties of these three regimes by studying the condensate first-order correlation function, the momentum distribution, and the distribution of the phase and density fluctuations. In the weakly nonlinear limit, we report evidence of an algebraic decay of the first-order correlation function indicating the emergence of the EW universality class, from which we establish, upon increasing the interaction strength a slow crossover towards stretched exponential decay with exponents of the 2d KPZ class, and eventually a very rapid decay leading to saturation in the vortex phase. This observed behaviors in the EW and KPZ regimes are then confirmed by a careful study of finite size effects in the condensate decoherence time. The different phases are also distinguished by their momentum distribution, where notably the EW and KPZ regimes exhibit different scaling at small momenta, in contrast with 1d condensates.

Finally, we have focused on the statistical properties of phase fluctuations to provide a further validation of the three identified regimes. We have found that the distribution of phase fluctuations is Gaussian in the EW weakly nonlinear regime, it displays non-Gaussian tails

at stronger non-linearity in the KPZ regime, in agreement with those predicted by numerical simulations of interfaces in the 2d KPZ class, whereas the distribution is exponential in the vortex regime. Unexpectedly, we observe that the probability distribution of the density fluctuations is not Gaussian in the EW and KPZ regimes, whose explanation deserves further studies.

Our analysis highlights that earlier observations from experiments [84] and numerical simulations [34] correspond to the realization of the EW regime and provides a microscopic prediction for the observed power-law decays and the ratio of the corresponding exponents.

Our work provides a unified picture of the universal properties of 2d polariton condensates in various parameter regimes. In outlook, from the theoretical point of view, it would be of great interest to provide a quantitative prediction for the transition to the vortex regime, whose qualitative picture has been developed in Refs. [30, 31], as well as a deeper understanding of oscillations observed in density correlations. A theoretical explanation for the observed non-Gaussian statistics of the density fluctuations in the EW and KPZ regimes is also missing. Overall, our findings pave the way for further experimental explorations of the universal properties of driven-dissipative quantum systems.

## ACKNOWLEDGMENTS

We warmly thank Ivan Amelio, Marzena Szymańska, Harvey Weinberger and Vincent Rossetto for stimulating discussions. FH acknowledges support from the Laboratoire d'excellence LANEF in Grenoble (ANR-10-LABX-51-01), AM acknowledges funding from the Quantum-SOPHA ANR Project ANR-21-CE47-0009. LC acknowledges support from Institut Universitaire de France (IUF). DPD, QF, SR, and JB acknowledge support from the Paris Ile-de-France Region in the framework of DIM QuanTIP, the French RENATECH network, the H2020-FETFLAG project PhoQus (820392), the European Research Council via projects StG ARQADIA (949730) and AdG ANAPOLIS (101054448)

## Appendix A: Adiabatic Bogoliubov theory

In this appendix, we explicit the connection between the phase of the condensate and the height of a growing interface, by relating its phase-phase correlation function to the EW two-point correlator under the Bogoliubov approximation. Adapting the calculations of Ref. [82], as detailed below, we show how the finite size of the system affects the long time decoherence of the EP BEC.

Setting  $\hbar = 1$ , the condensate dynamical equations read

$$i\partial_t\psi = \left[ \mathcal{F}^{-1} \left[ \epsilon_{\hat{\mathbf{k}}} - \frac{i}{2}\gamma_\ell(\hat{\mathbf{k}}) \right] + \frac{iR}{2}n_R + g|\psi|^2 + 2g_R n_R \right] \psi + \xi \quad (\text{A1})$$

$$\partial_t n_R = P - (\gamma_R + R|\psi|^2) n_R, \quad (\text{A2})$$

where  $\langle \xi \rangle = 0$  and  $\langle \xi(\mathbf{r}, t) \xi^*(\mathbf{r}', t') \rangle = 2\sigma\delta(\mathbf{r} - \mathbf{r}')\delta(t - t')$ .

In the adiabatic approximation of the reservoir  $\partial_t n_R \approx 0$ , Eq. (A2) reduces to  $n_R = P/(\gamma_R + R|\psi|^2)$ . The condensate wavefunction is expanded in fluctuations  $\delta\psi$  around its stationary mean field density  $n_0 = \gamma_R(p-1)/R$ , which reads  $\psi(\mathbf{r}, t) = e^{-i\Omega_0 t} [\sqrt{n_0} + \delta\psi(\mathbf{r}, t)]$ . Injecting it in Eq. (A1) leads at zeroth order to the mean field exciton reservoir density and condensate blueshift, respectively  $n_{R0} = \gamma_0/R$  and  $\Omega_0 = gn_0 + 2g_R n_{R0}$ . To first order in  $\delta\psi$ , Eq. (A1) reduces to the linear dynamics

$$i\partial_t \begin{pmatrix} \delta\psi \\ \delta\psi^* \end{pmatrix} = \mathcal{F}^{-1} [\mathcal{L}] \begin{pmatrix} \delta\psi \\ \delta\psi^* \end{pmatrix} + \sqrt{\sigma} \begin{pmatrix} \tilde{\xi} \\ -\tilde{\xi} \end{pmatrix} \quad (\text{A3})$$

where we introduced  $\tilde{\xi} = \xi e^{-i\Omega_0 t}$  and the Bogoliubov matrix

$$\mathcal{L} = \begin{pmatrix} \epsilon_{\hat{\mathbf{k}}} + g_e n_0 + i\Gamma_{\hat{\mathbf{k}}} & g_e n_0 - ig_i n_0 \\ -g_e n_0 - ig_i n_0 & -(\epsilon_{\hat{\mathbf{k}}} + g_e n_0) - i\Gamma_{\hat{\mathbf{k}}} \end{pmatrix} \quad (\text{A4})$$

with  $\Gamma_{\hat{\mathbf{k}}} = g_i n_0 + \frac{\Delta\gamma(\hat{\mathbf{k}})}{2}$ ,  $\Delta\gamma(\hat{\mathbf{k}}) = \gamma_\ell(\hat{\mathbf{k}}) - Rn_{R0}$  and  $g_i = \gamma_0^2/2P$ .

We introduce the rotation matrix

$$\mathcal{R} = \frac{1}{2\sqrt{n_0}} \begin{pmatrix} 1 & 1 \\ -i & i \end{pmatrix} \quad (\text{A5})$$

such that

$$\begin{pmatrix} \delta n/2n_0 \\ \delta\theta \end{pmatrix} = \mathcal{R} \begin{pmatrix} \delta\psi \\ \delta\psi^* \end{pmatrix} \quad (\text{A6})$$

and

$$(\partial_t - \mathcal{F}^{-1} [\mathcal{L}_{rot}]) \begin{pmatrix} \delta n/2n_0 \\ \delta\theta \end{pmatrix} = \sqrt{\frac{\sigma}{n_0}} \begin{pmatrix} \text{Im} \begin{pmatrix} \tilde{\xi} \\ \tilde{\xi} \end{pmatrix} \\ -\text{Re} \begin{pmatrix} \tilde{\xi} \\ \tilde{\xi} \end{pmatrix} \end{pmatrix} \quad (\text{A7})$$

with

$$\mathcal{L}_{rot} = \begin{pmatrix} -g_i n_0 - \Gamma_{\hat{\mathbf{k}}} & \epsilon_{\hat{\mathbf{k}}} \\ -(\epsilon_{\hat{\mathbf{k}}} + 2g_e n_0) & g_i n_0 - \Gamma_{\hat{\mathbf{k}}} \end{pmatrix}. \quad (\text{A8})$$

The eigenvalues of this matrix display the characteristic double-branched spectrum

$$\omega_{\pm} = i\Gamma_{\hat{\mathbf{k}}} \pm \sqrt{E_{\hat{\mathbf{k}}}^2 - g_i^2 n_0^2}, \quad (\text{A9})$$

with  $E_{\hat{\mathbf{k}}}^2 = \epsilon_{\hat{\mathbf{k}}}(\epsilon_{\hat{\mathbf{k}}} + 2g_e n_0)$ .

## 1. Phase-phase correlator

Within this approximation, the phase correlation reads in Fourier space

$$\langle \delta\theta_{\mathbf{k},\omega} \delta\theta_{-\mathbf{k},-\omega} \rangle = \frac{4\sigma g_e n_0 (\epsilon_{\hat{\mathbf{k}}} + g_e n_0) - g_i n_0 \Gamma_{\hat{\mathbf{k}}}}{n_0 (\omega^2 - \omega_-^2)(\omega^2 - \omega_+^2)} + \frac{\langle \delta n_{\mathbf{k},\omega} \delta n_{-\mathbf{k},-\omega} \rangle}{4n_0^2}. \quad (\text{A10})$$

The large scale properties of the condensate can be understood taking advantage of the splitting between these two branches at the crossover momentum  $k_c = \sqrt{2n_0|m|} \left[ \sqrt{g_e^2 + g_i^2} - |g_e| \right]^{1/2}$ , separating the infrared collective modes  $k \ll k_c$  from the ultraviolet free particles  $k \gg k_c$ . Focusing on the former limit and choosing  $\epsilon_{\hat{\mathbf{k}}} = k^2/2m$  and  $\gamma_\ell(\hat{\mathbf{k}}) = \gamma_0 + \gamma_2 k^2$ , we find for  $k \approx 0$  that  $\omega_+ \approx 2ig_i n_0$  and  $\omega_- \approx i\nu k^2$ , where  $\nu$  is the effective phase viscosity (4) introduced in the main text.

Under the condition that  $k \ll \sqrt{2g_i n_0/\nu}$  (for small  $\mu_{\text{th}}$ ,  $\sqrt{2g_i n_0/\nu} \sim 10k_c$ ), the real space two-point correlation function  $C_{\theta\theta}(r, t) = \langle [\delta\theta(\mathbf{r}, t) - \delta\theta(\mathbf{0}, 0)]^2 \rangle$  reads in generic dimension  $d$

$$\begin{aligned} C_{\theta\theta}(r, t) &\approx C_{\text{EW}}(r, t) - \frac{C_{nn}(r, t)}{2n_0^2} \\ &- 2D \int \frac{d\mathbf{k}}{(2\pi)^d} \frac{1 - e^{i\mathbf{k}\cdot\mathbf{r} - 2g_i n_0 t}}{2g_i n_0} \\ &+ \frac{8\sigma g_i n_0 \nu}{n_0} \int \frac{d\mathbf{k} d\omega}{(2\pi)^{d+1}} (1 - e^{i(\omega t + \mathbf{k}\cdot\mathbf{r})}) \\ &\times \frac{k^2}{(\omega^2 + 4g_i^2 n_0^2)(\omega^2 + \nu^2 k^4)} \end{aligned} \quad (\text{A11})$$

where  $C_{nn}(r, t) = \langle \delta n(r, t) \delta n(0, 0) \rangle - \langle \delta n(0, 0)^2 \rangle$ . The first term, which is the Edwards-Wilkinson two-point correlation defined by (A12), dominates the scaling behavior of  $C_{\theta\theta}(r, t)$  at short momenta. This is verified after integrating over frequencies, as the EW contribution reduces to  $\sim \int dk/k$  for  $d = 2$  while other terms contribute as  $\int k dk$  and  $\int k^2 dk$  which are subleading around  $k = 0$ . The EW correlation reads [2, 44]

$$C_{\text{EW}}(r, t) = C_0 t^{2\beta} F^{(d)} \left( \frac{r}{y_0 t^{1/z}} \right) \quad (\text{A12})$$

where  $C_0 = \frac{D}{\nu} (4\nu)^{2\beta}$  and  $y_0 = 2\sqrt{\nu}$  are non-universal constants, with  $D$  and  $\nu$  the effective parameters defined in Eqs. (4) and (6). This function is characterized by the universal dynamical exponent  $z = 2$ , the growth exponent  $\beta = \frac{2-d}{4}$ , and the universal scaling function  $F^{(d)}(y) = \int \frac{d\mathbf{k}}{(2\pi)^d} \frac{1 - e^{i\mathbf{k}\cdot\mathbf{y} - k^2/4}}{k^2}$  [44, 101].

Let us analyze the finite-size effects on  $C_{\text{EW}}(r = 0, t)$ . For a system of linear size  $L$ , from the diffusive nature of EW modes, one expects a change in its behavior at a time  $t^* \sim L^2/\nu$ . Following the arguments given in Ref. [82], we

can split the dimensionless momentum integral of  $F^{(d)}(y)$  into two: one for  $k^2 < 4$  (where  $e^{-k^2/4}$  is expanded to second order), the other for  $k^2 > 4$  (where  $e^{-k^2/4} \approx 0$ ). Reintroducing the dimensions, we can then take the short or long time limits of each of them, from which we obtain:

- *in dimension  $d = 1$* :  $C_{\text{EW}}(0, t \ll t^*) \approx \frac{2D}{\pi} \sqrt{t/\nu}$  consistent with the scale invariant form (A11). In the limit  $t \gg t^*$ ,  $C_{\text{EW}}(0, t) \approx \frac{4D}{\mathcal{L}} t$  where  $\mathcal{L}$  is a length scale maintaining homogeneity. A natural choice for this length scale, stemming from the lowest momenta of the finite-size system, is  $\mathcal{L} = \tau^{(1)} L$ , with  $\tau^{(1)}$  a dimensionless constant [86]. This constant contains the dependence of the condensate linewidth on the microscopic parameters that goes beyond the Bogoliubov approximation.

- *in dimension  $d = 2$* : Similarly we obtain for  $t \ll t^*$  that  $C_{\text{EW}}(0, t) \approx \frac{D}{2\pi\nu} [1 + \ln(\nu t \Lambda^2)]$ , *i.e.* a logarithmic time dependence [44, 55, 64, 65, 102] with  $\Lambda$  a momentum cutoff. When  $t \gg t^*$ ,  $C_{\text{EW}}(0, t) \approx \frac{D}{\tau^{(2)} L^2} t$  with the dimensionless constant  $\tau^{(2)}$ .

Overall, these results derived from the microscopic model reveal that Edwards-Wilkinson universal properties fully explain the decoherence of the condensate reported in the main text for small  $\mu_{\text{th}}$ . They can be recasted under the following scaling form

$$C_{\theta\theta}(0, t) \sim t^{2\beta} f^{(d)} \left( \frac{t}{L^z} \right). \quad (\text{A13})$$

with  $f^{(d)}(y) \underset{y \rightarrow +\infty}{\sim} y^{1-2\beta}$  for any dimensions, while the limit  $f^{(d)}(y \rightarrow 0)$  depends on it as suggested in Ref. [71]. The scaling form (A13) was found to also hold when  $\lambda \neq 0$ , in numerical simulations of 1d systems, where the exponents  $z$  and  $\beta$  are those of the KPZ class [85, 86].

From this finite-size study, we expect  $g^{(1)}(t \gg t^*) \sim e^{-t/\tau_c(L)}$  with the coherence time  $\tau_c(L) \propto L^{z-2\beta z}$ , generalizing the result of [86, 103] to 2d systems. This Schawlow-Townes-like limit [87], following EW or KPZ features, means that the growing phase interface loses the memory of its initial condition at long times and saturates to a Brownian motion [88].

## 2. Momentum distribution

From Eq. (A3) after integrating over frequencies, we immediately get the momentum distribution  $n_{\hat{\mathbf{k}}} = \langle \psi^*(\hat{\mathbf{k}}, t) \psi(\hat{\mathbf{k}}, t) \rangle$  as

$$n_{\hat{\mathbf{k}}} = 2\pi n_0 \delta(\mathbf{k}) + \frac{\sigma}{\Gamma_{\hat{\mathbf{k}}}} \left[ 1 + 4n_0^2 \frac{g_e^2 + g_i^2}{E_{\hat{\mathbf{k}}}^2 + \Gamma_{\hat{\mathbf{k}}}^2 - g_i^2 n_0^2} \right]. \quad (\text{A14})$$

Replacing  $\epsilon_{\hat{\mathbf{k}}} = k^2/2m$  and  $\gamma_\ell(\hat{\mathbf{k}}) = \gamma_0 + \gamma_2 k^2$ , we obtain  $n_{\hat{\mathbf{k}}} \underset{k \rightarrow +\infty}{\sim} \sigma/\gamma_2 k^2$  in the ultraviolet regime.



The short-momentum behavior is given, up to a constant, by  $n_{\mathbf{k}} \underset{k \rightarrow 0^+}{\sim} \tilde{C}_{\text{EW}}(k, t = 0)$ , where  $\tilde{C}_{\text{EW}}(k, t) = \int d\mathbf{r} e^{-i\mathbf{k}\cdot\mathbf{r}} C_{\text{EW}}(\mathbf{r}, t)$ .

At equal time, we obtain  $\tilde{C}_{\text{EW}}(k, 0) \sim k^{-2\beta z - d}$ . From this, we deduce that in the EW regime  $n_{\mathbf{k}} \propto k^{-2}$ . Since this result was obtained using the linear theory, we can expect the non-linearity of the phase dynamics to affect this regime and rather lead to  $n_{\mathbf{k}} \underset{k \rightarrow 0^+}{\sim} \tilde{C}_{\text{KPZ}}(k, t =$

$0) \sim k^{-2\beta z - d}$  with the KPZ exponents instead, giving  $n_{\mathbf{k}} \propto k^{-2.77}$ . This naive guess coincides with the KPZ asymptotic behavior observed in simulations of the noisy Kuramoto-Sivashinsky equation [104], as well as with predictions from acoustic turbulence in a 2d superfluid Bose gas [105]

Note that for  $d = 1$ , both EW and KPZ universality classes produce the same low-momentum power-law decay  $n_{\mathbf{k}} \propto 1/k^2$ , as confirmed by numerical simulations [26], which is no longer the case in 2d.

- 
- [1] H. Hinrichsen, Non-equilibrium critical phenomena and phase transitions into absorbing states, *Advances in Physics* **49**, 815–958.
- [2] S. Edwards and D. Wilkinson, The surface statistics of a granular aggregate, *Proceedings of the Royal Society of London. A. Mathematical and Physical Sciences* **381**, 17 (1982).
- [3] Y. Kuramoto, Diffusion-induced chaos in reaction systems, *Progress of Theoretical Physics Supplement* **64**, 346 (1978).
- [4] G. Sivashinsky, Nonlinear analysis of hydrodynamic instability in laminar flames—i. derivation of basic equations, *Acta Astronautica* **4**, 1177 (1977).
- [5] I. S. Aranson and L. Kramer, The world of the complex Ginzburg-Landau equation, *Reviews of Modern Physics* **74**, 99 (2002).
- [6] K. Sneppen, J. Krug, M. H. Jensen, C. Jayaprakash, and T. Bohr, Dynamic scaling and crossover analysis for the Kuramoto-Sivashinsky equation, *Physical Review A* **46**, R7351 (1992).
- [7] K. Ji, V. N. Gladilin, and M. Wouters, Temporal coherence of one-dimensional nonequilibrium quantum fluids, *Phys. Rev. B* **91**, 045301 (2015).
- [8] Q. Mei, K. Ji, and M. Wouters, Spatiotemporal scaling of two-dimensional nonequilibrium exciton-polariton systems with weak interactions, *Phys. Rev. B* **103**, 045302 (2021).
- [9] F. Helluin, L. Canet, and A. Minguzzi, Beyond mean-field corrections to the blueshift of a driven-dissipative exciton-polariton condensate, *Phys. Rev. B* **109**, 195304 (2024).
- [10] D. Forster, D. R. Nelson, and M. J. Stephen, Long-time tails and the large-eddy behavior of a randomly stirred fluid, *Phys. Rev. Lett.* **36**, 867 (1976).
- [11] M. Kardar, G. Parisi, and Y.-C. Zhang, Dynamic scaling of growing interfaces, *Phys. Rev. Lett.* **56**, 889 (1986).
- [12] K. A. Takeuchi, An appetizer to modern developments on the Kardar-Parisi-Zhang universality class, *Physica A: Statistical Mechanics and its Applications* **504**, 77 (2018), lecture Notes of the 14th International Summer School on Fundamental Problems in Statistical Physics.
- [13] T. Halpin-Healy and K. Takeuchi, A KPZ cocktail shaken, not stirred: Toasting 30 years of kinetically roughened surfaces, *J. Stat. Phys* **160**, 794 (2015).
- [14] M. A. C. Huergo, M. A. Pasquale, P. H. González, A. E. Bolzán, and A. J. Arvia, Growth dynamics of cancer cell colonies and their comparison with noncancerous cells, *Phys. Rev. E* **85**, 011918 (2012).
- [15] M. Žnidarič, Spin transport in a one-dimensional anisotropic heisenberg model, *Phys. Rev. Lett.* **106**, 220601 (2011).
- [16] N. Keenan, N. F. Robertson, T. Murphy, S. Zhuk, and J. Goold, Evidence of Kardar-Parisi-Zhang scaling on a digital quantum simulator, *npj Quantum Information* **9**, 72 (2023).
- [17] S. Mu, J. Gong, and G. Lemarié, Kardar-Parisi-Zhang physics in the density fluctuations of localized two-dimensional wave packets, *Phys. Rev. Lett.* **132**, 046301 (2024).
- [18] E. Altman, L. M. Sieberer, L. Chen, S. Diehl, and J. Toner, Two-dimensional superfluidity of exciton polaritons requires strong anisotropy, *Phys. Rev. X* **5**, 011017 (2015).
- [19] I. Carusotto and C. Ciuti, Quantum fluids of light, *Rev. Mod. Phys.* **85**, 299 (2013).
- [20] L. M. Sieberer, M. Buchhold, J. Marino, and S. Diehl, Universality in driven open quantum matter (2023), arXiv:2312.03073 [cond-mat.stat-mech].
- [21] L. M. Sieberer, M. Buchhold, and S. Diehl, Keldysh field theory for driven open quantum systems, *Reports on Progress in Physics* **79**, 096001 (2016).
- [22] D. Squizzato, L. Canet, and A. Minguzzi, Kardar-Parisi-Zhang universality in the phase distributions of one-dimensional exciton-polaritons, *Phys. Rev. B* **97**, 195453 (2018).
- [23] K. Deligiannis, D. Squizzato, A. Minguzzi, and L. Canet, Accessing Kardar-Parisi-Zhang universality sub-classes with exciton polaritons(a), *Europhysics Letters* **132**, 67004 (2021).
- [24] Q. Fontaine, D. Squizzato, F. Baboux, I. Amelio, A. Lemaître, M. Morassi, I. Sagnes, L. Le Gratiet, A. Harouri, M. Wouters, I. Carusotto, A. Amo, M. Richard, A. Minguzzi, L. Canet, S. Ravets, and J. Bloch, Kardar-Parisi-Zhang universality in a one-dimensional polariton condensate, *Nature* **608**, 687 (2022).
- [25] L. He, L. M. Sieberer, and S. Diehl, Space-time vortex driven crossover and vortex turbulence phase transition in one-dimensional driven open condensates, *Phys. Rev. Lett.* **118**, 085301 (2017).
- [26] F. Vercesi, Q. Fontaine, S. Ravets, J. Bloch, M. Richard, L. Canet, and A. Minguzzi, Phase diagram of one-dimensional driven-dissipative exciton-polariton condensates, *Phys. Rev. Res.* **5**, 043062 (2023).
- [27] V. L. Berezinsky, Destruction of long range order in one-dimensional and two-dimensional systems having a

- continuous symmetry group. I. Classical systems, Sov. Phys. JETP **32**, 493 (1971).
- [28] J. M. Kosterlitz and D. J. Thouless, Long range order and metastability in two dimensional solids and superfluids. (application of dislocation theory), Journal of Physics C: Solid State Physics **5**, L124 (1972).
- [29] D. Caputo, D. Ballarini, G. Dagvadorj, C. Sánchez Muñoz, M. De Giorgi, L. Dominici, K. West, L. N. Pfeiffer, G. Gigli, F. P. Laussy, M. Szymańska, and D. Sanvitto, Topological order and thermal equilibrium in polariton condensates, Nature Materials **17**, 145 (2018).
- [30] L. M. Sieberer, G. Wachtel, E. Altman, and S. Diehl, Lattice duality for the compact Kardar-Parisi-Zhang equation, Phys. Rev. B **94**, 104521 (2016).
- [31] G. Wachtel, L. M. Sieberer, S. Diehl, and E. Altman, Electrodynamical duality and vortex unbinding in driven-dissipative condensates, Phys. Rev. B **94**, 104520 (2016).
- [32] V. N. Gladilin and M. Wouters, Interaction and motion of vortices in nonequilibrium quantum fluids, New Journal of Physics **19**, 105005 (2017).
- [33] V. N. Gladilin and M. Wouters, Multivortex states and dynamics in nonequilibrium polariton condensates, Journal of Physics A: Mathematical and Theoretical **52**, 395303 (2019).
- [34] P. Comaron, I. Carusotto, M. H. Szymańska, and N. P. Proukakis, Non-equilibrium Berezinskii-Kosterlitz-Thouless transition in driven-dissipative condensates(a), Europhysics Letters **133**, 17002 (2021).
- [35] G. Dagvadorj, M. Kulczykowski, M. H. Szymańska, and M. Matuszewski, First-order dissipative phase transition in an exciton-polariton condensate, Phys. Rev. B **104**, 165301 (2021).
- [36] E. Altman, L. M. Sieberer, L. Chen, S. Diehl, and J. Toner, Two-dimensional superfluidity of exciton polaritons requires strong anisotropy, Phys. Rev. X **5**, 011017 (2015).
- [37] A. Zamora, L. M. Sieberer, K. Dunnett, S. Diehl, and M. H. Szymańska, Tuning across universalities with a driven open condensate, Phys. Rev. X **7**, 041006 (2017).
- [38] L. M. Sieberer and E. Altman, Topological defects in anisotropic driven open systems, Phys. Rev. Lett. **121**, 085704 (2018).
- [39] A. Zamora, N. Lad, and M. H. Szymanska, Vortex dynamics in a compact Kardar-Parisi-Zhang system, Phys. Rev. Lett. **125**, 265701 (2020).
- [40] A. Ferrier, A. Zamora, G. Dagvadorj, and M. H. Szymańska, Searching for the Kardar-Parisi-Zhang phase in microcavity polaritons, Phys. Rev. B **105**, 205301 (2022).
- [41] G. Dagvadorj, J. M. Fellows, S. Matyjaśkiewicz, F. M. Marchetti, I. Carusotto, and M. H. Szymańska, Nonequilibrium phase transition in a two-dimensional driven open quantum system, Phys. Rev. X **5**, 041028 (2015).
- [42] F. Baboux, D. D. Bernardis, V. Goblot, V. N. Gladilin, C. Gomez, E. Galopin, L. L. Gratiet, A. Lemaitre, I. Sagnes, I. Carusotto, M. Wouters, A. Amo, and J. Bloch, Unstable and stable regimes of polariton condensation, Optica **5**, 1163 (2018).
- [43] C. Schneider, K. Winkler, M. D. Fraser, M. Kamp, Y. Yamamoto, E. A. Ostrovskaya, and S. Höfling, Exciton-polariton trapping and potential landscape engineering, Reports on Progress in Physics **80**, 016503 (2016).
- [44] T. Nattermann and L.-H. Tang, Kinetic surface roughening. I. the Kardar-Parisi-Zhang equation in the weak-coupling regime, Phys. Rev. A **45**, 7156 (1992).
- [45] M. Wouters and I. Carusotto, Excitations in a nonequilibrium bose-einstein condensate of exciton polaritons, Phys. Rev. Lett. **99**, 140402 (2007).
- [46] M. Wouters and V. Savona, Stochastic classical field model for polariton condensates, Phys. Rev. B **79**, 165302 (2009).
- [47] J. Kasprzak, M. Richard, S. Kundermann, A. Baas, P. Jeambrun, J. Keeling, F. Marchetti, M. Szymańska, R. André, J. Staehli, V. Savona, P. B. Littlewood, B. Deveaud, and L. S. Dang, Bose-Einstein condensation of exciton polaritons, Nature **443**, 409 (2006).
- [48] E. Medina, T. Hwa, M. Kardar, and Y.-C. Zhang, Burgers equation with correlated noise: Renormalization-group analysis and applications to directed polymers and interface growth, Phys. Rev. A **39**, 3053 (1989).
- [49] G. Ódor, B. Liedke, and K.-H. Heinig, Directed  $d$ -mer diffusion describing the Kardar-Parisi-Zhang-type surface growth, Phys. Rev. E **81**, 031112 (2010).
- [50] J. Kelling and G. Ódor, Extremely large-scale simulation of a Kardar-Parisi-Zhang model using graphics cards, Phys. Rev. E **84**, 061150 (2011).
- [51] A. Pagnani and G. Parisi, Numerical estimate of the Kardar-Parisi-Zhang universality class in  $(2+1)$  dimensions, Phys. Rev. E **92**, 010101 (2015).
- [52] E. Perlsman and M. Schwartz, The directed polymer problem in general dimension, Physica A: Statistical Mechanics and its Applications **234**, 523 (1996).
- [53] J. M. Kim, M. A. Moore, and A. J. Bray, Zero-temperature directed polymers in a random potential, Phys. Rev. A **44**, 2345 (1991).
- [54] J. M. Kim and J. M. Kosterlitz, Growth in a restricted solid-on-solid model, Phys. Rev. Lett. **62**, 2289 (1989).
- [55] L.-H. Tang, B. M. Forrest, and D. E. Wolf, Kinetic surface roughening. II. Hypercube-stacking models, Phys. Rev. A **45**, 7162 (1992).
- [56] I. S. S. Carrasco and T. J. Oliveira, Kardar-Parisi-Zhang growth on square domains that enlarge nonlinearly in time, Phys. Rev. E **105**, 054804 (2022).
- [57] T. J. Oliveira, Kardar-Parisi-Zhang universality class in  $(d + 1)$ -dimensions, Phys. Rev. E **106**, L062103 (2022).
- [58] L. Canet, H. Chaté, B. Delamotte, and N. Wschebor, Nonperturbative renormalization group for the Kardar-Parisi-Zhang equation: General framework and first applications, Phys. Rev. E **84**, 061128 (2011).
- [59] T. Halpin-Healy,  $(2+1)$ -dimensional directed polymer in a random medium: Scaling phenomena and universal distributions, Phys. Rev. Lett. **109**, 170602 (2012).
- [60] T. Halpin-Healy, Extremal paths, the stochastic heat equation, and the three-dimensional Kardar-Parisi-Zhang universality class, Phys. Rev. E **88**, 042118 (2013).
- [61] T. J. Oliveira, S. G. Alves, and S. C. Ferreira, Kardar-Parisi-Zhang universality class in  $(2 + 1)$  dimensions: Universal geometry-dependent distributions and finite-time corrections, Phys. Rev. E **87**, 040102 (2013).
- [62] I. S. S. Carrasco, K. A. Takeuchi, S. C. Ferreira, and T. J. Oliveira, Interface fluctuations for deposition on enlarging flat substrates, New Journal of Physics **16**, 123057 (2014).

- [63] I. Corwin, The Kardar - Parisi - Zhang equation and universality class, *Random matrices: Theory and applications* **1**, 1130001 (2012).
- [64] B. M. Forrest and L.-H. Tang, Hypercube stacking: A Potts-spin model for surface growth, *Journal of Statistical Physics* **60**, 181 (1990).
- [65] S. Pal and D. Landau, The Edwards–Wilkinson model revisited: large-scale simulations of dynamic scaling in 2+1 dimensions, *Physica A: Statistical Mechanics and its Applications* **267**, 406 (1999).
- [66] I. S. Aranson and L. Kramer, The world of the complex ginzburg-landau equation, *Rev. Mod. Phys.* **74**, 99 (2002).
- [67] H. Chaté and P. Manneville, Phase diagram of the two-dimensional complex ginzburg-landau equation, *Physica A: Statistical Mechanics and its Applications* **224**, 348 (1996), dynamics of Complex Systems.
- [68] J. M. Hyman, B. Nicolaenko, and S. Zaleski, Order and complexity in the Kuramoto-Sivashinsky model of weakly turbulent interfaces, *Physica D: Nonlinear Phenomena* **23**, 265 (1986).
- [69] R. Cuerno and K. B. Lauritsen, Renormalization-group analysis of a noisy Kuramoto-Sivashinsky equation, *Physical Review E* **52**, 4853 (1995).
- [70] P. Manneville and H. Chaté, Phase turbulence in the two-dimensional complex Ginzburg-Landau equation, *Physica D: Nonlinear Phenomena* **96**, 30 (1996), measures of Spatio-Temporal Dynamics.
- [71] G. Grinstein, C. Jayaprakash, and R. Pandit, Conjectures about phase turbulence in the complex Ginzburg-Landau equation, *Physica D: Nonlinear Phenomena* **90**, 96 (1996).
- [72] D. Roy and R. Pandit, One-dimensional kardar-parisi-zhang and kuramoto-sivashinsky universality class: Limit distributions, *Phys. Rev. E* **101**, 030103 (2020).
- [73] F. Vercesi, S. Poirier, A. Minguzzi, and L. Canet, Scaling regimes of the one-dimensional phase turbulence in the deterministic complex ginzburg-landau equation, *Phys. Rev. E* **109**, 064149 (2024).
- [74] I. Aranson, L. Kramer, and A. Weber, Core instability and spatiotemporal intermittency of spiral waves in oscillatory media, *Phys. Rev. Lett.* **72**, 2316 (1994).
- [75] I. S. Aranson, H. Chaté, and L.-H. Tang, Spiral motion in a noisy complex ginzburg-landau equation, *Phys. Rev. Lett.* **80**, 2646 (1998).
- [76] K. Deligiannis, Q. Fontaine, D. Squizzato, M. Richard, S. Ravets, J. Bloch, A. Minguzzi, and L. Canet, Kardar-Parisi-Zhang universality in discrete two-dimensional driven-dissipative exciton polariton condensates, *Phys. Rev. Res.* **4**, 043207 (2022).
- [77] G. P. Agrawal, Chapter 2 - fiber couplers, in *Applications of Nonlinear Fiber Optics (Second Edition)* (Academic Press, Burlington, 2008) second edition ed., pp. 54–99.
- [78] L. A. Smirnov, D. A. Smirnova, E. A. Ostrovskaya, and Y. S. Kivshar, Dynamics and stability of dark solitons in exciton-polariton condensates, *Phys. Rev. B* **89**, 235310 (2014).
- [79] T. C. H. Liew, O. A. Egorov, M. Matuszewski, O. Kyriienko, X. Ma, and E. A. Ostrovskaya, Instability-induced formation and nonequilibrium dynamics of phase defects in polariton condensates, *Phys. Rev. B* **91**, 085413 (2015).
- [80] A. J. Bray, A. J. Briant, and D. K. Jervis, Breakdown of scaling in the nonequilibrium critical dynamics of the two-dimensional  $XY$  model, *Phys. Rev. Lett.* **84**, 1503 (2000).
- [81] A. Chiocchetta and I. Carusotto, Non-equilibrium quasi-condensates in reduced dimensions, *Europhysics Letters* **102**, 67007 (2013).
- [82] J. Keeling, M. H. Szymańska, and P. B. Littlewood, Keldysh green's function approach to coherence in a non-equilibrium steady state: connecting bose-einstein condensation and lasing, in *Optical Generation and Control of Quantum Coherence in Semiconductor Nanostructures*, edited by G. Slavcheva and P. Rousignol (Springer Berlin Heidelberg, Berlin, Heidelberg, 2010) pp. 293–329.
- [83] G. Roumpos, M. Lohse, W. H. Nitsche, J. Keeling, M. H. Szymanska, P. B. Littlewood, A. Löffler, S. Höfling, L. Worschech, A. Forchel, and Y. Yamamoto, Power-law decay of the spatial correlation function in exciton-polariton condensates, *Proc Natl Acad Sci U S A* **109**, 6467 (2012).
- [84] P. Comaron, E. Estrecho, M. Wurdack, M. Pieczarka, M. Steger, D. W. Snoke, K. West, L. N. Pfeiffer, A. G. Truscott, M. Matuszewski, M. Szymanska, and E. A. Ostrovskaya, Coherence of a non-equilibrium polariton condensate across the interaction-mediated phase transition (2024), arXiv:2407.10506 [cond-mat.quant-gas].
- [85] J. Krug, Origins of scale invariance in growth processes, *Advances in Physics* **46**, 139 (1997), <https://doi.org/10.1080/00018739700101498>.
- [86] I. Amelio, A. Chiocchetta, and I. Carusotto, Kardar-Parisi-Zhang universality in the coherence time of nonequilibrium one-dimensional quasicondensates, *Phys. Rev. E* **109**, 014104 (2024).
- [87] A. L. Schawlow and C. H. Townes, Infrared and optical masers, *Phys. Rev.* **112**, 1940 (1958).
- [88] G. Grynberg, A. Aspect, and C. Fabre, Complement 3d: The spectral width of a laser: the Schawlow–Townes limit, in *Introduction to Quantum Optics: From the Semi-classical Approach to Quantized Light* (Cambridge University Press, 2010) p. 257–260.
- [89] J. Krug and P. Meakin, Universal finite-size effects in the rate of growth processes, *Journal of Physics A: Mathematical and General* **23**, L987 (1990).
- [90] K. A. Takeuchi, Statistics of circular interface fluctuations in an off-lattice eden model, *Journal of Statistical Mechanics: Theory and Experiment* **2012**, P05007 (2012).
- [91] K. A. Takeuchi, Crossover from growing to stationary interfaces in the Kardar-Parisi-Zhang class, *Phys. Rev. Lett.* **110**, 210604 (2013).
- [92] K. A. Takeuchi and M. Sano, Universal fluctuations of growing interfaces: Evidence in turbulent liquid crystals, *Phys. Rev. Lett.* **104**, 230601 (2010).
- [93] K. A. Takeuchi and M. Sano, Evidence for geometry-dependent universal fluctuations of the Kardar-Parisi-Zhang interfaces in liquid-crystal turbulence, *Journal of Statistical Physics* **147**, 853 (2012).
- [94] T. Iwatsuka, Y. T. Fukai, and K. A. Takeuchi, Direct evidence for universal statistics of stationary Kardar-Parisi-Zhang interfaces, *Phys. Rev. Lett.* **124**, 250602 (2020).
- [95] Y. T. Fukai and K. A. Takeuchi, Kardar-Parisi-Zhang interfaces with curved initial shapes and variational formula, *Phys. Rev. Lett.* **124**, 060601 (2020).

- [96] R. A. L. Almeida, S. O. Ferreira, T. J. Oliveira, and F. D. A. A. a. Reis, Universal fluctuations in the growth of semiconductor thin films, *Phys. Rev. B* **89**, 045309 (2014).
- [97] T. Halpin-Healy and G. Palasantzas, Universal correlators and distributions as experimental signatures of (2+1)-dimensional Kardar-Parisi-Zhang growth, *Europhysics Letters* **105**, 50001 (2014).
- [98] R. A. L. Almeida, S. O. Ferreira, I. Ferraz, and T. J. Oliveira, Initial pseudo-steady state & asymptotic KPZ universality in semiconductor on polymer deposition, *Scientific Reports* **7**, 3773 (2017).
- [99] D. Roy and R. Pandit, One-dimensional Kardar-Parisi-Zhang and Kuramoto-Sivashinsky universality class: Limit distributions, *Phys. Rev. E* **101**, 030103 (2020).
- [100] W. Liu and U. C. Täuber, Nucleation of spatiotemporal structures from defect turbulence in the two-dimensional complex Ginzburg-Landau equation, *Phys. Rev. E* **100**, 052210 (2019).
- [101] A. Barabási and H. Stanley, *Fractal concepts in surface growth* (Cambridge university press, 1995).
- [102] A. Bray, Theory of phase-ordering kinetics, *Advances in Physics* **43**, 357 (1994).
- [103] I. Amelio and I. Carusotto, Bogoliubov theory of the laser linewidth and application to polariton condensates, *Phys. Rev. A* **105**, 023527 (2022).
- [104] M. Nicoli, E. Vivo, and R. Cuerno, Kardar-Parisi-Zhang asymptotics for the two-dimensional noisy Kuramoto-Sivashinsky equation, *Phys. Rev. E* **82**, 045202 (2010).
- [105] S. Mathey, T. Gasenzer, and J. M. Pawłowski, Anomalous scaling at nonthermal fixed points of Burgers' and Gross-Pitaevskii turbulence, *Phys. Rev. A* **92**, 023635 (2015).